pH-responsive nano-structured membranes prepared from oppositely charged block copolymer nanoparticles and iron oxide nanoparticles

Ujala Farooq, Lakshmeesha Upadhyaya, Ahmad Shakeel, Gema Martinez, M. Semsarilar

pH-Responsive Nano-Structured Membranes Prepared from Oppositely Charged Block Copolymer Nanoparticles and Iron Oxide Nanoparticles

Ujala Farooq[a§], *Lakshmeesha Upadhyaya*[a†], *Ahmad Shakeel*[b], *Gema Martinez*[c,d], *Mona Semsarilar*[a*]

[a] Institut Européen des Membranes, IEM, UMR 5635, Univ. Montpellier, CNRS, ENSCM, Montpellier, France.

[b] Faculty of Civil Engineering and Geosciences, Delft University of Technology, the Netherlands.

[c] Networking Research Centre on Bioengineering, Biomaterials and Nanomedicine, CIBER-BBN, 28029 Madrid, Spain.

[d] Department of Chemical and Environmental Engineering and Aragon Nanoscience Institute, Campus Río Ebro, C/ Mariano Esquillor s/n ,50018 Zaragoza, Spain.

[*] Corresponding author

Current address:

[§] Faculty of Aerospace Engineering, Delft University of Technology, the Netherlands.

[†] King Abdullah University of Science and Technology (KAUST), Biological and Environmental Science and Engineering Division, Advanced Membranes and Porous Materials Center, 23955-6900, Thuwal, Saudi Arabia.

Abstract

Nanostructured (hybrid) membranes combining properties of inorganic and polymeric materials is an integral part of the field of separation technology. Mixed matrix membranes were prepared from oppositely charged inorganic (INPs) and polymeric (PNPs) nanoparticles using spin coating method. Four different types of PNPs were prepared. Poly(2-dimethylaminoethyl methacrylate)-*b*-(methyl methacrylate)) and poly((methacrylic acid)-*b*-(methyl methacrylate)) diblock copolymers were prepared via RAFT dispersion polymerization in ethanol at 70°C. Quaternized poly(2-(dimethylamino) ethyl

methacrylate)-*b*-poly (benzyl methacrylate) and poly(potassium 3-sulfopropyl methacrylate)-*b*-poly (benzyl methacrylate) block copolymers were prepared using aqueous RAFT emulsion polymerization method at 70°C. The inorganic iron oxide nanoparticles (INPs) were either coated with [3-(2-Aminoethylamino)propyl] trimethoxysilane (TPED) via Dimercaptosuccinic acid (DMSA) using stab exchange. Transmission electron microscopy (TEM) and Dynamic light scattering (DLS) analysis were performed to examine the size and morphology of the prepared polymeric and inorganic nanoparticles. Scanning electron microscope (SEM) and Atomic Force Microscope (AFM) images were obtained to analyze the topography and thin film formation on the nylon support. Detailed filtration experiments were carried out to evaluate the effect of pH on the performance of the membrane.

Keywords: pH-responsive membranes, Block copolymer nanoparticles, Iron oxide nanoparticles, Surface charge, SEM, AFM, Filtration

1. Introduction

Since the last few decades, polymeric membranes have played an essential role in separation and purification technologies. However, there are certain limitations of these membranes posed by their mechanical stability, particularly for thin-film membranes, and chemical resistant [1]. Mixed matrix membranes have been evolved as a potential alternative to polymeric membranes because of their superior mechanical properties by choosing suitable components [2, 3]. The fabrication method for such composite membranes consists of incorporation of inorganic nanoparticles into a polymeric matrix. Several types of inorganic materials have been reported so far in the literature to prepare these hybrid membranes including mesoporous materials [4], carbon nanotubes (CNTs) [5], zeolites [6, 7], metal-organic frameworks (MOFs) [8], and metal oxides [9, 10]. The most exciting feature of these hybrid membranes is that they exhibit merits of both phases (organic and inorganic materials), such as mechanical stability and pressure resistance comes from inorganic phase while flexibility, low cost, and processability results from the polymeric material [11]. Apart from giving higher mechanical stability, the incorporation of nanoparticles also provides other unusual characteristics such as photochemical, magnetic and antimicrobial properties, which results in advanced applications of such hybrid membranes [12].

A critical challenge for the advancement of membranes is to have higher permeability and reasonable selectivity in a single membrane. This challenge comes with the requirement of selective and thin-film membranes in addition to the high porosity and regular porous structure [13]. Amphiphilic block copolymers have gained so much attraction, as a potential solution to challenges mentioned above because of their capability to self-assemble into ordered nanostructures, i.e., porous materials [14, 15]. Pore size and structure of membrane can easily be tuned by playing with the type and morphology of block copolymers, which eventually tunes the flux, and the selectivity of the membranes. These fascinating self-assembling copolymers have increased the scope of application such as purification in food and pharmaceutical industry [16], water treatment [17], drug delivery [18], data storage [19] and

hemodialysis [20]. So far, different methods including extrusion, spin coating, and bulk evaporation have been developed to prepare membranes from block copolymers [21]. The major drawback of these methods is the requirement of post-fabrication steps to make porous structures in the thin films. Recently, this problem has been solved by combining two phenomena, self-assembly of block copolymers with the non-solvent induced phase separation (NIPS), to produce exceptionally isoporous asymmetric membranes without the need of any post-fabrication step to create porosity [22].

Recently, stimuli-responsive membranes have gained attention due to their switchable physicochemical and barrier properties [23]. These new membranes can modify their mass transfer and interfacial properties in response to the external stimuli including direct ones (i.e., pH, temperature and ionic strength [24, 25]) and newly developed remote or indirect triggers (i.e., light, magnetic and electric fields [26, 27]). The main objective for the preparation of stimuli-responsive membranes is to have the reversible changes in addition to the high selectivity at a faster rate. The conformational changes in the functional groups of responsive polymers, either in bulk membrane or at the surface, give rise to the stimulus response. The process of responsiveness in such membranes usually occurs in two steps [28]: (i) morphological changes in polymer, on microscopic level, in response to the stimuli (ii) intensification of these microscopic morphological transformations into macroscopic changes that can be measured as different membrane properties. As compared to other external stimuli, pH responsiveness provides more alternatives for materials and their application fields, making it a new and useful approach.

Zhang et al. [29] described the production of pH-sensitive membranes by mixing ethylcellulose with poly(N-isopropyl acrylamide-*co*-methacrylic acid) nanoparticles, produced via aqueous dispersion polymerization method. The prepared membranes were coated with the layers of polyelectrolyte to prevent the separation of nanoparticles from the membrane surface. Nunes et al. [30] prepared the pH-responsive membranes having self-assembly of metal-block copolymer complexes using NIPS technique. The structure of the thin film was manipulated by using different stability constants of series of metal-polymer complexes. The most vigorous pH response was evident for the membranes having pores of

nano-meter size. The effect of pH on the pore sizes of hybrid membranes was also reported by Tufani et al. [31]. These composite membranes were synthesized by the surface modification of the pore walls with pH-responsive block copolymer via initiated chemical vapor deposition (iCVD). pH responsiveness of the prepared membranes was tested under various pH values by using different permeates such as polyacrylic acid (PAA), nanoparticles, and BSA protein. Recently, Fan et al. [32] reported the development of pH sensitive smart gating membranes by efficiently incorporating poly(*N,N′*-dimethylamino-2-ethyl methacrylate) (PDMAEMA) microgels, as functional gates, into poly(ether sulfone) (PES) membrane through liquid-induced phase separation technique. The prepared membranes displayed positive pH-responsive behavior in an acidic environment whereas in a basic environment, negative pH-responsive behavior was evident.

Recently, we developed a novel method to synthesize thin-film membranes from sequential spray coating of self-assembled block copolymers nanoparticles [33]. Spray coating is a convenient approach to prepare thin layers involving two mechanisms, bulk movement in the spray and random spreading in the liquid film [34]. The anionic and cationic block copolymers were produced using Reversible Addition Fragmentation Chain Transfer (RAFT) aqueous emulsion polymerization method which, self-assembled spontaneously into spherical nanoparticles in the presence of water through polymerization induced self-assembly. The results revealed the fine-tuning of polymeric layer thickness by controlling the number of deposited layers. Formation of porous and defect free membranes was also confirmed by imaging analysis. In our previous studies [14, 35-37], we also reported the preparation of nanocomposite membranes with particular pore sizes, by using already produced colloidally stable solutions. By movement using this method, membrane of desired pore size could be easily synthesized by first preparing the nanoparticles of a particular diameter which will assemble to give a porous membrane with the desired properties. The final properties of the developed membranes were also manipulated by playing with the type of nanoparticles [14, 37]. We reported the preparation of nanocomposite membranes from block copolymer nanoparticles of different morphologies (worms, spheres, and vesicles) and

functionalized iron oxide nanoparticles [36]. The results showed a prominent effect of the amount of functionalized INPs and pH values on the mechanical stability of membranes. Application of the magnetic field also showed an increase in the flux due to the movement of the magneto-responsive iron oxide nanoparticles [37].

In this study, new strategies to prepare inorganic nanoparticles (INPs) and polymeric nanoparticles having positive and negative surface charges are being developed. Thin-film membranes are synthesized by the combination of positive inorganic nanoparticles (INPs) coated with [3-(2-Aminoethylamino)propyl] trimethoxysilane (TPED) and negative diblock copolymeric nanoparticles (PNPs) such as $PMAA_{64}$-$PMMA_{400}$ and by combining negative INPs coated with Dimercaptosuccinic acid (DMSA) and positive PNPs ($PDMAEMA_{80}$-$PMMA_{500}$). Another set of polymeric nanoparticles having positive and negative surface charges ($PQDMA_{23}$-$PBzMA_{300}$ and $PKSPMA_{36}$-$PBzMA_{300}$), previously prepared in our group [33], is also mixed with inorganic nanoparticles coated with the opposite charges to make thin-film membranes. In contrast to our previous studies, functionalization of INPs is done on the core of the particle instead of a polymeric chain on the surface. Furthermore, pH-sensitive (PMAA and PDMAEMA) and non-pH-sensitive (PQDMA and PKSPMA) block copolymer nanoparticles are utilized in this study to assess the effect of pH on the membrane performance. Using these four types of PNPs along with the two pH sensitive INPs allow preparation of membranes from PNP/ INP pairs where both nanoparticles are sensitive to pH as well as pairs that only the INP has pH sensitivity. This large combination of nanoparticles permits the preparation of pH sensitive membranes with different pore sizes and flux values. The nanoparticles are characterized by Transmission Electron Microscopy (TEM) and Dynamic Light Scattering (DLS). Nanocomposite membranes are analyzed by using Atomic Force Microscopy (AFM), Scanning Electron Microscopy (SEM), and filtration tests at different pH values.

2. Results and discussion

2.1. Synthesis and characterization of the block copolymer nanoparticles (PNPs) and inorganic nanoparticles (INPs)

In our previous study [36], we synthesized mixed matrix membranes from negatively charged PMAA-*b*-PMMA block copolymer particles with different morphologies (prepared through polymerization induced self-assembly) and positively charged iron oxide nanoparticles coated with quaternized poly(2-dimethylamino)ethyl methacrylate. The effect of particle morphology (spheres, worms, and vesicles), added amount of inorganic particles and pH values on filtration and mechanical performance of the prepared membranes were evaluated. It was demonstrated that the membranes from spherical NPs in the presence of high enough positively charged magnetic nanoparticles had the best performance with a pore size of 2−20 nm. The positively charged INPs increased the mechanical stability of the final membrane due to electrostatic attractions.

In this work, following a similar methodology, a library of charged spherical polymeric nanoparticles (pH-responsive and non-pH responsive) is prepared. Reversible Addition Fragmentation Chain Transfer (RAFT) ethanolic dispersion and aqueous emulsion polymerization methods are used to synthesize positively and negatively charged diblock copolymer nanoparticles through polymerization induced self-assembly (PISA) method. The cationic diblock copolymer particles are synthesized by using cationic steric stabilizer (macro-chain transfer agent) based on poly(2-dimethylaminoethyl methacrylate) (PDMAEMA), and a core-forming hydrophobic block based on poly(methyl methacrylate) (PMMA). The second cationic block copolymer nanoparticles are prepared by using a macro-chain transfer agent based on quaternized poly(2-(dimethylamino) ethyl methacrylate) (PQDMA), and a hydrophobic core based on poly(benzyl methacrylate) (PBzMA). On the other hand, the anionic diblock copolymer nanoparticles are prepared using an anionic stabilizer of PMAA, and a hydrophobic core of PMMA. Similarly, the second anionic copolymer nanoparticles were made from an anionic poly(potassium 3-sulfopropyl methacrylate) (PKSPMA) stabilizer and a hydrophobic core of PBzMA. All four block copolymer nanoparticles formed spherical nanoparticles in ethanol or water under polymerization induced self-assembly (PISA) regime.

DLS study of $PDMAEMA_{80}$-$PMMA_{500}$ nanoparticles presented broad size distribution and stable spheres with an average hydrodynamic diameter of 28.8 ± 1.3 nm with the polydispersity index of 0.9 and width of 25.5 ± 0.3 nm (from TEM analysis) (Fig. S1C). DLS investigation of $PMAA_{64}$-$PMMA_{400}$ nanoparticles

also indicated narrow size distribution, and stable spheres with an average hydrodynamic diameter of 22.8 ± 1.7 nm, the diameter of these nanoparticles from TEM investigation is about 18.9 ± 1.1 nm (Fig. S1D). Furthermore, $PMAA_{64}$-$PMMA_{400}$ baring negative surface charge, due to the presence of polymethacrylic acid groups on their surface, with a zeta potential of -38 ± 2.0 mV at pH 8. The $PDMAEMA_{80}$-$PMMA_{500}$ particles had positive surface charge (zeta potential value of 28.9± 5.0 mV at pH 8 (Table S1)) due to the presence of the amine groups. DLS measurements of $PQDMA_{23}$-$PBzMA_{300}$ nanoparticles revealed narrow size distribution and stable spheres with an average hydrodynamic diameter of 40 nm whereas a narrow size distribution and stable spheres with an average hydrodynamic diameter of 45 nm were obtained for $PKSPMA_{36}$-$PBzMA_{300}$ nanoparticles. TEM analysis showed a diameter of 26.4 ± 1.1 nm and 28.8 ± 0.5 nm for $PQDMA_{23}$-$PBzMA_{300}$ and $PKSPMA_{36}$-$PBzMA_{300}$ nanoparticles, respectively (Figs. S1E & S1F). The charged inorganic nanoparticles were synthesized via previously reported methods [39, 40]. Positively charged iron oxide nanoparticles bared amino groups (INPs-TPED), and the negatively charged particles had succinic acid groups on their surface (INPs-DMSA) (Fig. 1). DLS measurements of INPs-TPED nanoparticles showed narrow size distribution and solid spheres having an average hydrodynamic diameter of 57.4 nm. The TEM analysis of the nanoparticles proposed diameter of 3.1 nm (Fig. S1A). DLS characterization of INPs-DMSA also displayed narrow size distribution and stable spheres with an average hydrodynamic diameter of 25.4 nm, whereas the diameter from TEM analysis was 1.0 nm (Fig. S1B).

2.2.Synthesis and Characterization of Hybrid Membranes

To prepare the casting solutions, oppositely charged PNP and INP were mixed at different ratios (Fig. 1). To avoid precipitation of the oppositely charged nanoparticles, the isoelectric point (IEP) of each PNP/INP pair was determined, and the PNP: INP ratios were kept below the IEP of each pair (see Table 1). The casting solution mixtures were stirred at room temperature for 24h. This solution mixture was then vortexed 10-15 minutes before membrane casting. Spin coating was used to deposit a thin layer of

185 the nanoparticles on commercial nylon support with an average pore diameter of 0.2 µm. The prepared
186 hybrid membranes were analyzed using AFM, SEM and filtration test.

Table 1. Summary of amounts of nanoparticles required for preparation of the membrane casting solutions

Sample ID	Sample Membranes	Inorganic Nanoparticles (INPs)*				Polymeric Nanoparticles (PNPs)			
		Amount of INPs to get the isoelectric point (mL)		Amount of INPs to get the isoelectric point (mL)		Amount of PNPs to make membrane solution (mL)			
		Fe_3O_4-DMSA	Fe_3O_4-TPED	Fe_3O_4-DMSA	Fe_3O_4-TPED	$PDMAEMA_{80}$-$PMMA_{500}$	$PMAA_{64}$-$PMMA_{400}$	$PQDMA_{23}$-$PBzMA_{300}$	$PKSPMA_{36}$-$PBzMA_{300}$
HM1	$PMAA_{64}$-$PMMA_{400}$-Fe_3O_4-TPED	-	1.4	1.2	-	-	0.5	-	-
HM2	$PQDMA_{23}$-$PBzMA_{300}$-DMSA- Fe_3O_4	3.0	-	-	2.6	-	-	0.5	-
HM3	$PKSPMA_{36}$-$PBzMA_{300}$-TPED- Fe_3O_4	-	2.6	2.0	-	-	-	-	0.5
HM4	$PDMAEMA_{80}$ -$PMMA_{500}$-Fe_3O_4-DMSA	1.0	-	0.8	-	0.5	-	-	-

* Concentration of Fe_3O_4-DMSA stock solution = 2.14 mg/mL
* Concentration of Fe_3O_4-TPED stock solution = 1.27 mg/mL

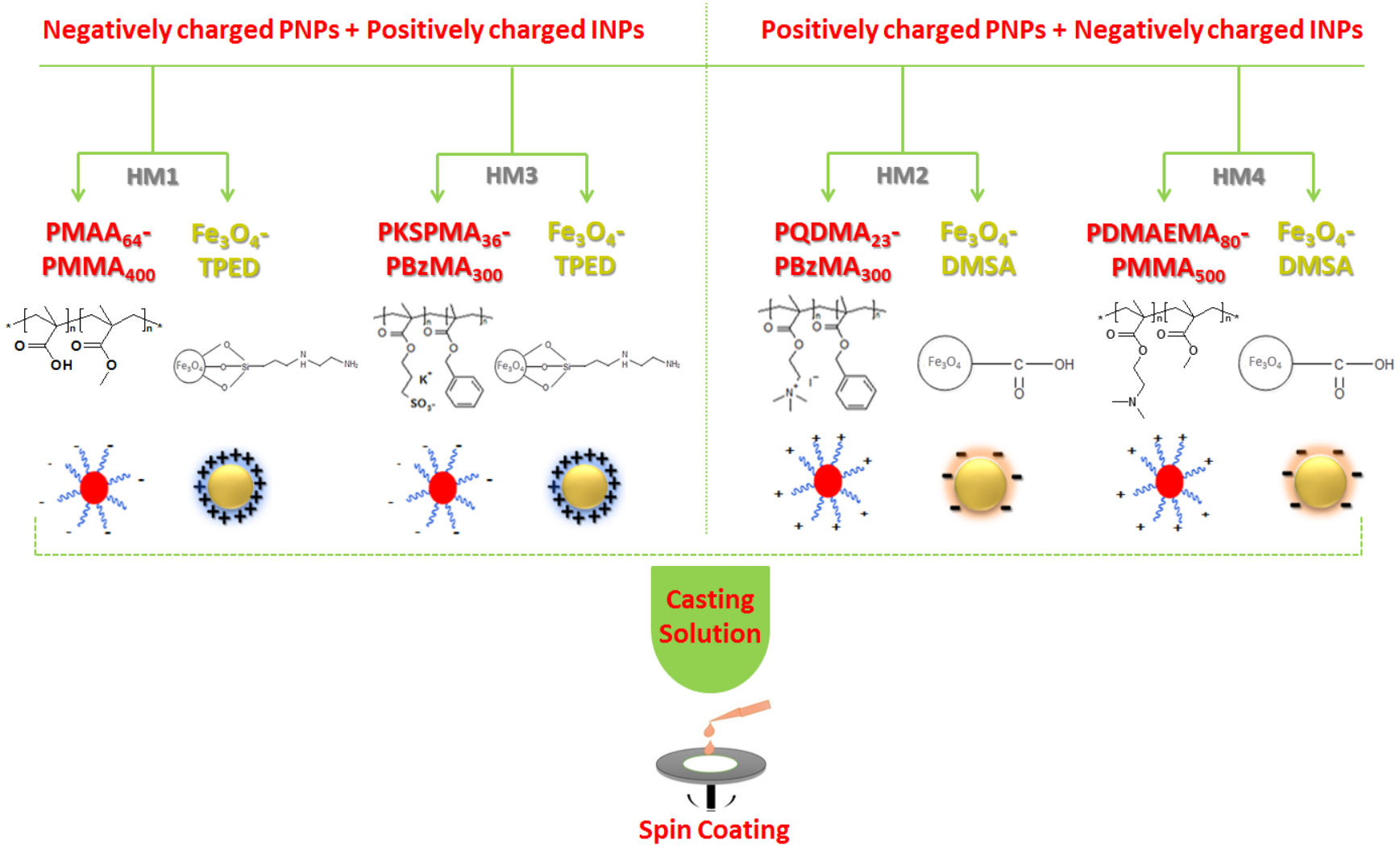

192

193 **Fig. 1.** Schematic representation of nanostructured membrane prepared from oppositely charged PNPs and INPs

Fig. 2 shows the topography of the prepared four nanostructured membranes. These AFM images clearly show the spherical morphology of the PNP nanoparticles and also confirm the compact packing of the PNPs with no visible alteration due to the presence of the INPs.

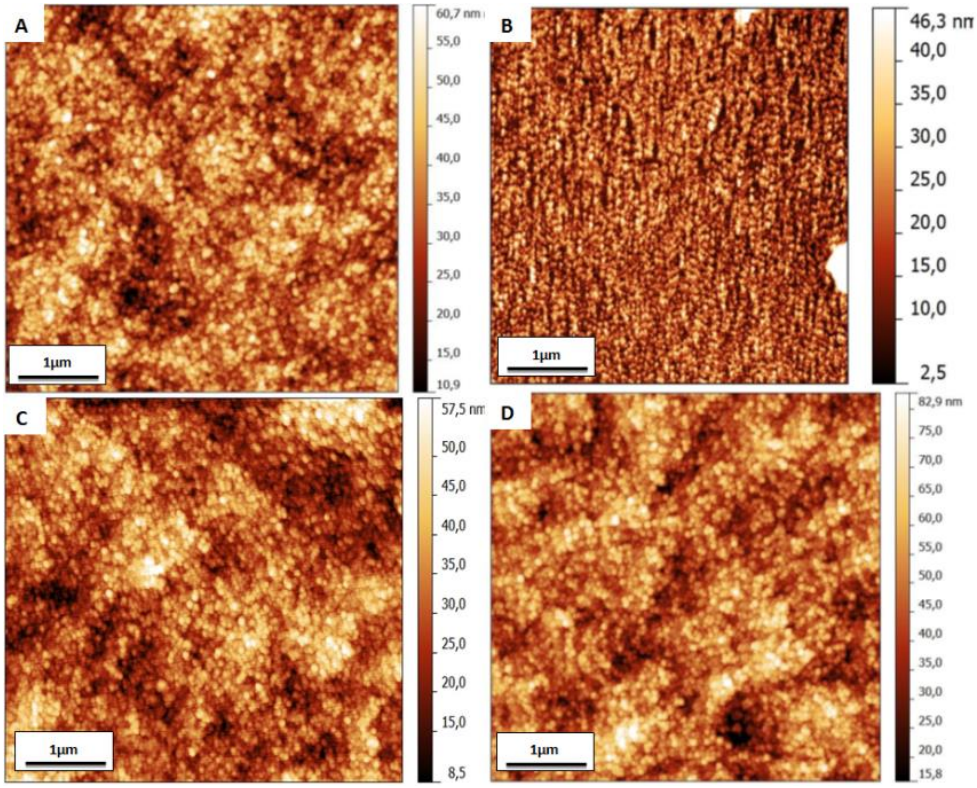

Fig. 2. Atomic force microscopic images of the membranes (A) HM1 (B) HM2 (C) HM3 and (D) HM4.

The SEM images of all four membranes (HM1-4, Fig. 3) display the formation of defect-free active layers. The thickness of the top layer of membrane containing $PMAA_{64}$-$PMMA_{400}$ and INPs-TPED is about 1.82 µm while membrane containing $PDMAEMA_{80}$-$PMMA_{500}$ and INPs-DMSA has top layer thickness of 1.84 µm. Similarly, $PQDMA_{23}$-$PBzMA_{300}$ and $PKSPMA_{36}$-$PBzMA_{300}$ nanoparticles based membranes have top layer thickness of 1.89 µm and 1.56 µm, respectively.

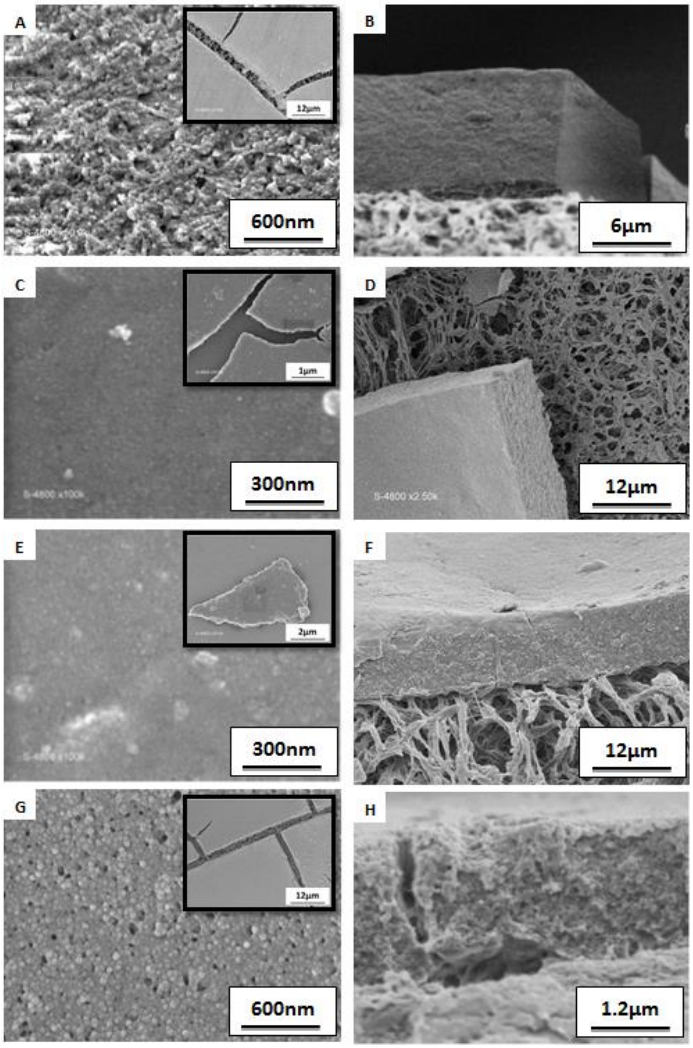

Fig. 3. SEM images of (A, C, E, and G) top surface and (B, D, F and H) cross-section of (A, B) HM1, (C, D) HM2, (E, F) HM3 and (G, H) HM4 membranes. Insets present the images of the top surface with lower magnification.

It is apparent that the void among the congested nanoparticles gives rise to the porous structure. Theoretical pore size was estimated using a straightforward model based on the hexagonal arrangement of mono-disperse spheres [35]. Here, the average diameter of the $PMAA_{64}$-$PMMA_{400}$ and $PDMAEMA_{80}$-$PMMA_{500}$ spherical nanoparticles are 18.9 nm and 25.5 nm, respectively as measured from TEM images. The calculated pore diameter is considered to be 0.4142 times of a sphere diameter (Fig. S2). The estimated pore size for HM1 membrane is 7.8 nm, while for HM4 membrane is 10.5 nm. By performing the same calculation, the estimated pore size for HM2 membrane is 10.9 nm, whereas for HM3 membrane this value is 11.9 nm (Table 2). The pore diameter calculations were based on particle diameters measured

from TEM images as the membranes are at semi-dry state; hence, the particle size should be closer to dry state rather than the hydrodynamic diameter at colloidal state. During the calculations, the INPs diameter was not considered since they are much smaller as compared to the PNPs. HM2 to HM4 membranes show similar pore size compared to HM1. The shells of the PNPs used in these membranes are made of permanently charged polymeric chains (strong poly-acid and base). The presence of permanent charge in a polymer chain forces them to be in an extended and rigid configuration rather than the entangled and collapsed state. In the block copolymer, the extended ionic block will be much more solvated compared to a collapsed polymeric chain resulting in the formation of more hydrated nanoparticle shell hence a bigger nanoparticle size and pore diameter.

Table 2. Theoretical pore sizes of the prepared membranes calculated using Eq. in Fig. S4.

Sample ID	PNPs size (nm)	Pore size (nm)
HM1	18.9	7.8
HM2	26.4	10.9
HM3	28.8	11.9
HM4	25.5	10.5

The prepared membranes were also tested for pure water filtration. The filtration cycles (repeated three times) were all performed on the same membrane. The membranes were fitted in a filtration cell with a diameter of 2.5 cm and a volume of 10 mL. Each membrane was conditioned for 2 hours at 3.5 bar, and then water flux was recorded to reach an equilibrium state. For filtration under pressure, the filtration cell was filled with water and linked with a pressurized water reservoir. Upon collection of data, Darcy's law was used to calculate the flux (J_v) and permeability (L_p) values using the following equations [41]:

$$J_v = \frac{V_p}{t\,S}$$

$$L_p = \frac{J_v}{\Delta P}$$

where, V_p corresponds to the volume of water going through the membrane (L), t represents time (h), S denotes the surface of the membrane (m^2), and ΔP is water pressure (bar).

Water flux (J_v) was calculated at different pressure intervals between 0 and 3.5 bar. At each pressure, 20 minutes equilibrium time was allowed before recording the data, followed by a 20 minutes recording. In all four cases, the water flux plots versus pressure show an almost linear increase (Figs. 5A, 4C, 4E & 5G). Figs. 5B, 5D, 5F, and 5H show that the permeability is almost constant as a function of applied pressure which also verifies the stability of the prepared membranes under tested conditions. For HM4 membrane, at 3.5 bar the calculated flux was 50.8 L/hm^2 and the resultant permeability was 36.2 L/hm^2bar whereas for HM1 membrane, at 3.5 bar the calculated flux was 7.69 L/h.m^2, and the resultant permeability was 4.60 L/hm^2bar. In the same way, for HM3 membrane, at 3.5 bar the calculated flux was 18.7 L/hm^2 with the permeability of 4.52 L/hm^2bar and for HM2 membrane, at 3.5 bar the calculated flux is 18.3 L/hm^2 with the permeability of 5.34 L/hm^2bar. These flux values were lower than the values already reported in literature for PMAA-PMMA based membranes having PMAA-*b*-PQDMAEMA coated INPs [36, 37] which may be due to the fact that the INPs used in this study are stabilized using small molecules as compared to the INPs used in the previous study which had hairy shell structure (stabilized with positively charged polymer chains with an average size of 7 nm). These particles were less prone to aggregation because of the presence of the charged polymer chain. However, the INPs stabilized using only an acid or amine group (INP-DMSA and INP-TPED) aggregated readily as it could be seen from the data presented in Table S1. The average size measured from TEM images (dry state) show particle diameters of 1 and 3 nm for the negatively and positively charged particles respectively. While DLS measurements in solution, gave diameters of 25 and 57 nm for the same particles. Such a big difference is size could only be due to particle aggregation. Therefore, if the INPs present in the membrane dope solutions are aggregated (i.e. larger diameters) they would possibly clog some of the

membrane pores reducing the apparent pore size, resulting in lower flux values. This aggregation could also be the reason behind the small hysteresis observed in the flux curves. If the INPs are aggregated, they would interact less with the polymer chains stabilizing the PNPs. This could influence the cohesion of the particles brought about by the electrostatic forces due to the presence of oppositely charged nanoparticles. Weaker cohesion would lead to lower stability of the membrane active layer that could be slightly pushed into the support layer under water pressure (during filtration).

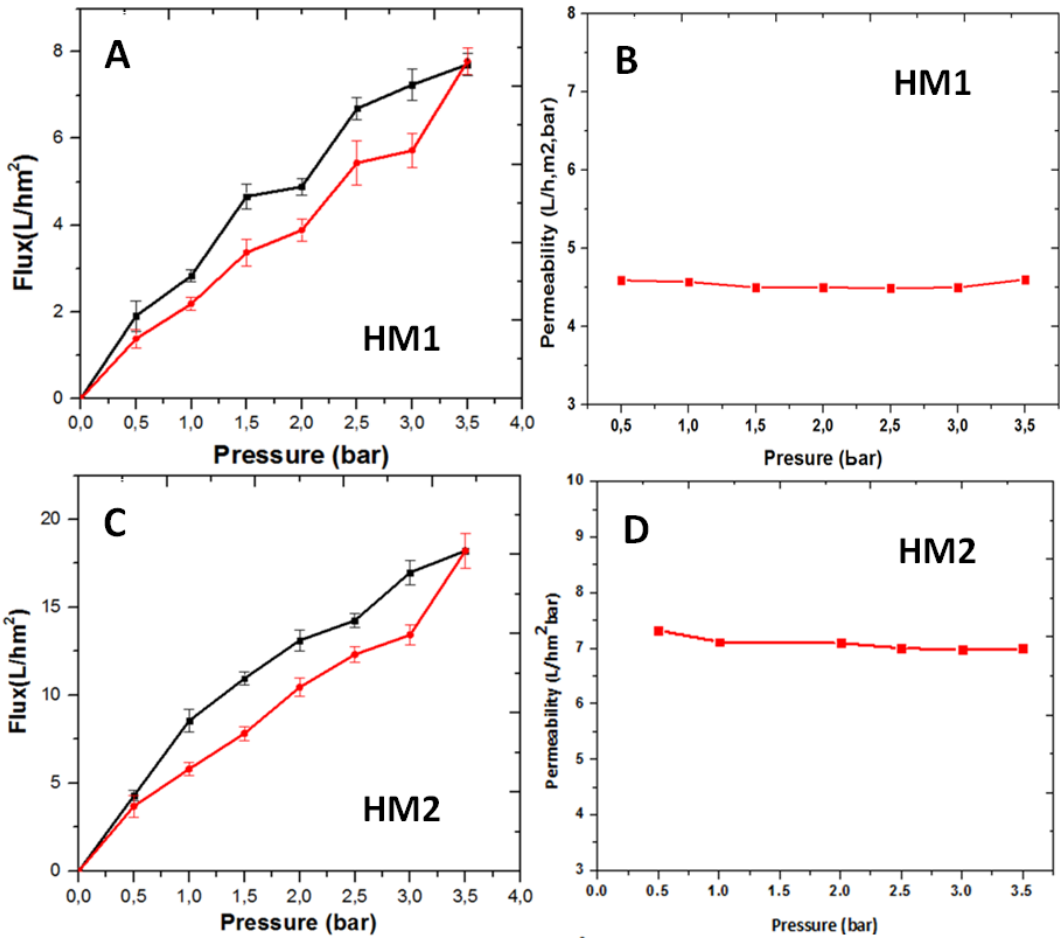

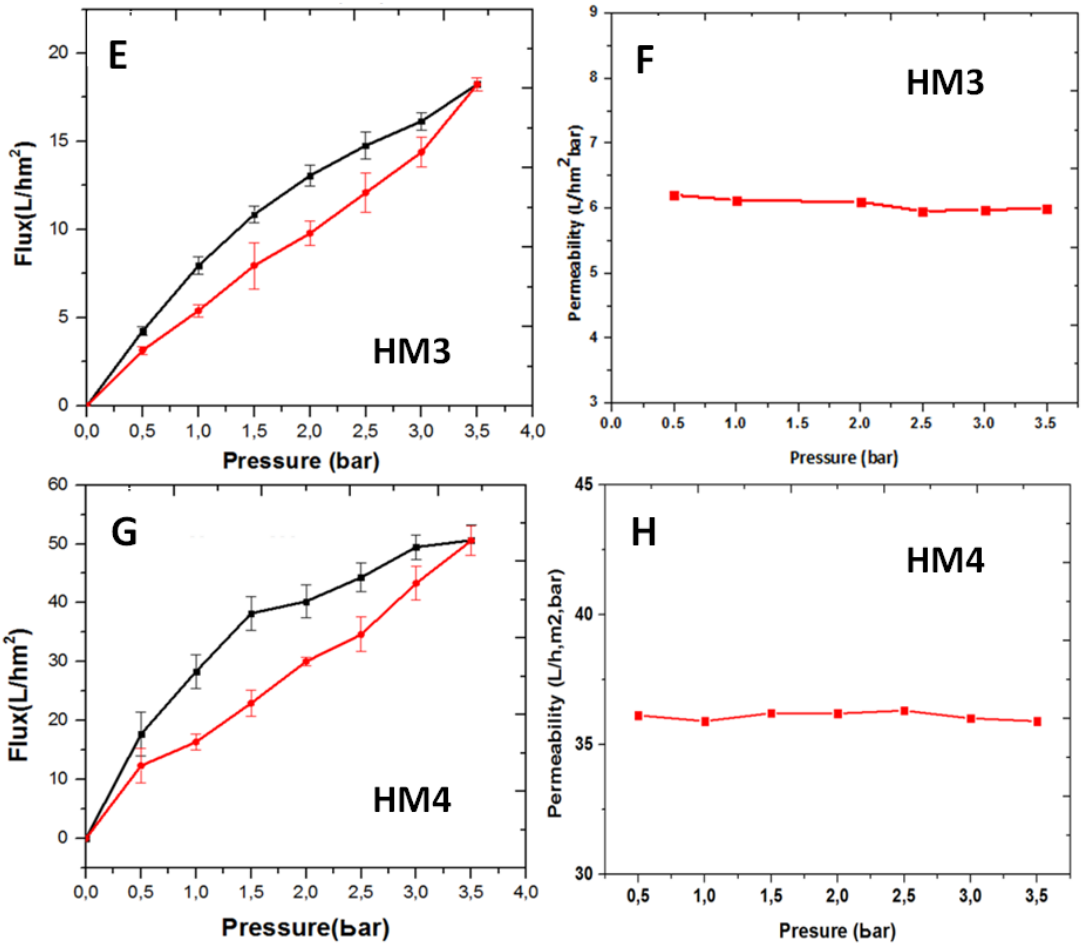

Fig. 5. (A, C, E, and G) Water flux (J_v) and (B, D, F, and H) Permeability (L_p) as a function of pressure for nanostructured membranes (A, B) HM1 (C, D) HM2 (E, F) HM3 and (G, H) HM4 at pH of 7. The reported values are the average of three different measurements, and the bars represent the standard deviation. Blackline is pressure ramp up, and the red is the ramp down.

$PMAA_{64}$-$PMMA_{400}$ and $PDMAEMA_{80}$-$PMMA_{500}$ polymeric nanoparticles are pH-sensitive because of the presence of PMAA and PDMAEMA on their surface. So are the inorganic nanoparticles used, as they bear either –COOH (DMSA, pKa 1 = 2.9, pKa 2 = 4.5) or $–NH_2$ (TPED, pKa = 8) functionalities. To see the effect of the pH change on the pore size of the nanostructured membranes, filtration tests at acidic and basic pH values were performed. Feed solutions with pH values below and above the pK_a of PDMAEMA and PMAA (7.4-7.8 and 6.1, respectively) [36, 42] were used for filtration (pH 2 and 10). The flux shows the increasing trend as a function of applied pressure for both acidic and basic pH values (Fig. 6A-H).

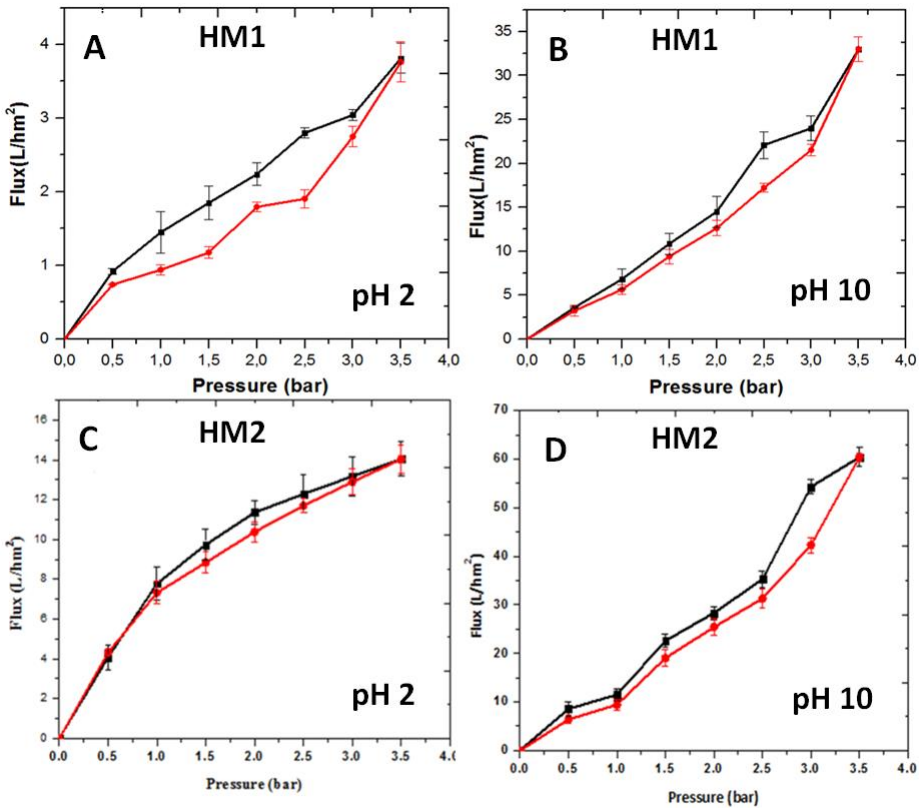
A
HM1
pH 2
Flux(L/hm²)
Pressure (bar)
B
HM1
pH 10
Flux(L/hm²)
Pressure (bar)
C
HM2
pH 2
Flux (L/hm²)
Pressure (bar)
D
HM2
pH 10
Flux (L/hm²)
Pressure (bar)

278

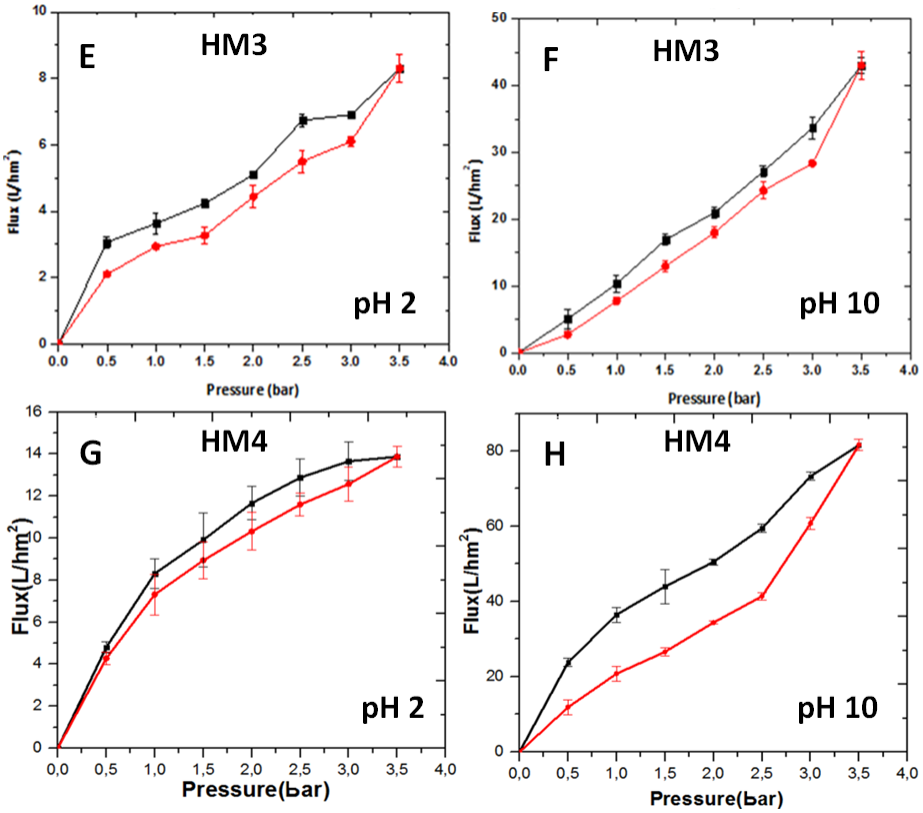
E
HM3
pH 2
Flux (L/hm²)
Pressure (bar)
F
HM3
pH 10
Flux (L/hm²)
Pressure (bar)
G
HM4
pH 2
Flux(L/hm²)
Pressure(bar)
H
HM4
pH 10
Flux(L/hm²)
Pressure(bar)

279

Fig. 6. Water flux (J_v) as a function of pressure for (A, B) HM1 membranes, (C, D) HM2 membranes, (E, F) HM3 membranes and (G, H) HM4 membranes, at (A, C, E and G) pH 2 and (B, D, F and H) pH 10. The values are the average of three different measurements, and the bars represent the standard deviation. Blackline is pressure ramp up, and the red is a ramp down.

The flux increases progressively from 3.5 L/hm^2 at 1.0 bar to 34.6 L/hm^2 at 3.5 bar for pH 10 in case of HM1, while for HM4 membrane flux increases gradually from 22.3 L/hm^2 at 1 bar to 81.2 L/hm^2 at 3.5 bar for pH 10. Likewise, the flux increases from 11.5 L/hm^2 at 1.0 bar to 60.4 L/hm^2 at 3.5 bar for pH 10 in case of HM2, whereas for HM3 membrane flux increases from 10.33 L/hm^2 at 1 bar to 43.03 L/hm^2 at 3.5 bar for pH 10. The SEM analysis of hybrid membranes was also performed after filtration tests and the micrographs revealed no signs of deformation on the active layer (Fig. S5).

To be able to compare the membranes together, the maximum flux values recorded at 3 different pH (2, 7 and 10) at 3.5 bar were plotted in one single figure (Fig. 7). The flux values were at lowest when the water pH was 2. The flux values are lower for prepared membranes at pH 2 as compared to the values at pH 10. This is because at pH 2 there is only a small number of charges present since pH 2 is below the pKa of all the used functional nanoparticles (PNP and INP). As the number of apparent charge on the surface of the nanoparticles increase (pH $\geq$ 10) the flux value increases sharply. This is most likely due to the repulsive forces generated between the packed particles forcing them to move. This stands out more in membranes made from nanoparticles coated with PDMAEMA as stabilizer (with highest flux values at all 3 pH values tested). For this nanoparticle pair (PDMAEMA-PMMA and INP-DMSA) there is no pH value where both particles are charged. This means that the cohesion between the PNP particles is at its minimum due to same charge repulsion.

The changes in flux brought about by pH could be very useful to tune the pore size according to the filtration regime/ range. If membrane with bigger pore size is required a cycle of filtration with water at pH 10 could be performed prior to the actual sample filtration. Another simple method to tune the pore size would be to soak the membrane in water with a certain pH value.

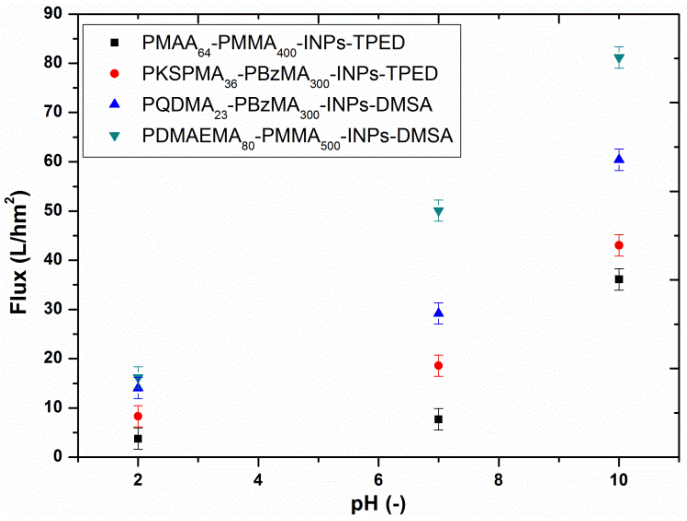

Fig. 7. Water flux as a function of pH for different nanostructured membranes at 3.5 bar. Black color represents $PMAA_{64}$-$PMMA_{400}$-INPs-TPED (HM1 membrane), red color represents $PKSPMA_{36}$-$PBzMA_{300}$-INPs-TPED (HM3 membrane), blue color represents $PQDMA_{23}$-$PBzMA_{300}$-INPs-DMSA (HM2 membrane) and green color represents $PDMAEMA_{80}$-$PMMA_{500}$-INPs-TPED (HM4 membrane).

Conclusion

In summary, iron oxide nanoparticles were prepared by polyol method and functionalized with [3-(2-Aminoethylamino)propyl] trimethoxysilane (TPED) and Dimercaptosuccinic acid (DMSA) to achieve the positive and negative charges on their surface. $PDMAEMA_{80}$-$PMMA_{500}$ and $PMAA_{64}$-$PMMA_{400}$ copolymer nanoparticles were prepared via RAFT-PISA synthesis method in ethanol while $PKSPMA_{36}$-$PBzMA_{300}$ and $PQDMA_{23}$-$PBzMA_{300}$ copolymer nanoparticles in water. High conversions were attained within 24 hours. DLS analysis showed their spherical features, and TEM images represented well-defined nanoparticles. Cationic and anionic nanoparticle pairs were effectively utilized to synthesize thin-film membranes by spin coating method on a nylon support. SEM and AFM analysis revealed the formation of porous and defect-free membranes. Pressure–driven water filtration tests, using prepared membranes, were performed at different pH values. Since the pK_a value of polymethacrylic acid (PMAA) on the surface of PNPs is about 6.1 and for PDMAEMA on the surface is in the range of 7.4-7.8, therefore, feed solutions of two different pH values, 2 and 10, were used and the filtration experiments were performed. For neutral pH (7), the membranes HM1 displayed the flux of 7.69 L/hm^2, while HM4 membranes

showed the flux of 50.8 L/hm^2 at 3.5 bar of pressure. In the same way, for HM3 membranes, at 3.5 bar, the flux was 15.4 L/hm^{2,} and for HM2 membranes, at 3.5 bars, the calculated flux was 21.3 L/hm^2. The highest recorded flux was 81.2 L/hm^2 for HM4 nanostructured membranes at the pressure of 3.5 bars and pH 10, which was linked with the deprotonation of the amine groups resulted in higher water flux. When the pH value was below the pK_a value (pH 2) lower flux values were observed for all the investigated membranes which were attributed to the existence of a fewer number of charges for interaction. The filtration tests also verified the mechanical stability of studied membranes under the investigated pressure range (0-3.5 bars). The prepared nanostructure membranes were found to have a pore size in a nano-metric range following lower limit of ultrafiltration and upper limit of nano-filtration. The adequate bonding of positively and negatively charged particles (PNPs and INPs) resulted in the enhanced mechanical stability of the prepared membranes. In future work, the magneto-responsive behavior of these hybrid membranes can further be examined.

Acknowledgments

U. F. acknowledges the financial support from EM3E Master Programme, which is an Educational Programme supported by the European Commission, the European Membrane Society (EMS), the European Membrane House (EMH), and an extensive international network of industrial companies, research centers and universities. The authors would like to thank Dr. Reyes Mallada for the fruitful discussions and for the help in preparing this manuscript.

References

[1] D.J. Kim, M.J. Jo, S.Y. Nam, A review of polymer–nanocomposite electrolyte membranes for fuel cell application, Journal of Industrial and Engineering Chemistry, 21 (2015) 36-52.

[2] A.K. Singh, P. Singh, S. Mishra, V.K. Shahi, Anti-biofouling organic-inorganic hybrid membrane for water treatment, Journal of Materials Chemistry, 22 (2012) 1834-1844.

[3] Y. Gu, R.M. Dorin, U. Wiesner, Asymmetric organic–inorganic hybrid membrane formation via block copolymer–nanoparticle co-assembly, Nano letters, 13 (2013) 5323-5328.

[4] B. Zornoza, C. Téllez, J. Coronas, Mixed matrix membranes comprising glassy polymers and dispersed mesoporous silica spheres for gas separation, Journal of Membrane Science, 368 (2011) 100-109.

[5] P. Goh, A. Ismail, B. Ng, Carbon nanotubes for desalination: Performance evaluation and current hurdles, Desalination, 308 (2013) 2-14.

[6] M. Jia, K.-V. Peinemann, R.-D. Behling, Molecular sieving effect of the zeolite-filled silicone rubber membranes in gas permeation, Journal of Membrane Science, 57 (1991) 289-292.

[7] H.H. Yong, H.C. Park, Y.S. Kang, J. Won, W.N. Kim, Zeolite-filled polyimide membrane containing 2, 4, 6-triaminopyrimidine, Journal of Membrane Science, 188 (2001) 151-163.

[8] S. Basu, A. Cano-Odena, I.F. Vankelecom, MOF-containing mixed-matrix membranes for CO_2/CH_4 and CO_2/N_2 binary gas mixture separations, Separation and Purification Technology, 81 (2011) 31-40.

[9] P. Jian, H. Yahui, W. Yang, L. Linlin, Preparation of polysulfone–Fe_3O_4 composite ultrafiltration membrane and its behavior in magnetic field, Journal of Membrane Science, 284 (2006) 9-16.

[10] S. Matteucci, V.A. Kusuma, D. Sanders, S. Swinnea, B.D. Freeman, Gas transport in TiO_2 nanoparticle-filled poly (1-trimethylsilyl-1-propyne), Journal of Membrane Science, 307 (2008) 196-217.

[11] M.M. Pendergast, E.M. Hoek, A review of water treatment membrane nanotechnologies, Energy & Environmental Science, 4 (2011) 1946-1971.

[12] P. Madhavan, P.-Y. Hong, R. Sougrat, S.P. Nunes, Silver-enhanced block copolymer membranes with biocidal activity, ACS applied materials & interfaces, 6 (2014) 18497-18501.

[13] G. Dong, H. Li, V. Chen, Challenges and opportunities for mixed-matrix membranes for gas separation, Journal of Materials Chemistry A, 1 (2013) 4610-4630.

[14] L. Upadhyaya, M. Semsarilar, R. Fernández-Pacheco, G. Martinez, R. Mallada, A. Deratani, D. Quemener, Porous membranes from acid decorated block copolymer nano-objects via RAFT alcoholic dispersion polymerization, Polymer Chemistry, 7 (2016) 1899-1906.

[15] L. Upadhyaya, M. Semsarilar, S. Nehache, A. Deratani, D. Quemener, Filtration membranes from self-assembled block copolymers–a review on recent progress, The European Physical Journal Special Topics, 224 (2015) 1883-1897.

[16] S.Y. Yang, J.-A. Yang, E.-S. Kim, G. Jeon, E.J. Oh, K.Y. Choi, S.K. Hahn, J.K. Kim, Single-file diffusion of protein drugs through cylindrical nanochannels, Acs Nano, 4 (2010) 3817-3822.

[17] M.A. Shannon, P.W. Bohn, M. Elimelech, J.G. Georgiadis, B.J. Marinas, A.M. Mayes, Science and technology for water purification in the coming decades, Nature, 452 (2008) 301-310.

[18] E.A. Jackson, M.A. Hillmyer, Nanoporous membranes derived from block copolymers: from drug delivery to water filtration, ACS nano, 4 (2010) 3548-3553.

[19] T. Thurn-Albrecht, J. Schotter, G. Kästle, N. Emley, T. Shibauchi, L. Krusin-Elbaum, K. Guarini, C. Black, M. Tuominen, T. Russell, Ultrahigh-density nanowire arrays grown in self-assembled diblock copolymer templates, Science, 290 (2000) 2126-2129.

[20] I. Hamley, Nanostructure fabrication using block copolymers, Nanotechnology, 14 (2003) R39-R54.

[21] D. Wu, F. Xu, B. Sun, R. Fu, H. He, K. Matyjaszewski, Design and preparation of porous polymers, Chemical reviews, 112 (2012) 3959-4015.

[22] S.P. Nunes, A. Car, From charge-mosaic to micelle self-assembly: block copolymer membranes in the last 40 years, Industrial & Engineering Chemistry Research, 52 (2012) 993-1003.

[23] C. Zhao, S. Nie, M. Tang, S. Sun, Polymeric pH-sensitive membranes—a review, Progress in Polymer Science, 36 (2011) 1499-1520.

[24] S. Frost, M. Ulbricht, Thermoresponsive ultrafiltration membranes for the switchable permeation and fractionation of nanoparticles, Journal of membrane science, 448 (2013) 1-11.
[25] T. Ito, T. Hioki, T. Yamaguchi, T. Shinbo, S.-i. Nakao, S. Kimura, Development of a molecular recognition ion gating membrane and estimation of its pore size control, Journal of the American Chemical Society, 124 (2002) 7840-7846.
[26] T. Hoare, B.P. Timko, J. Santamaria, G.F. Goya, S. Irusta, S. Lau, C.F. Stefanescu, D. Lin, R. Langer, D.S. Kohane, Magnetically triggered nanocomposite membranes: a versatile platform for triggered drug release, Nano letters, 11 (2011) 1395-1400.
[27] B.P. Timko, T. Dvir, D.S. Kohane, Remotely triggerable drug delivery systems, Advanced materials, 22 (2010) 4925-4943.
[28] D. Wandera, S.R. Wickramasinghe, S.M. Husson, Stimuli-responsive membranes, Journal of Membrane Science, 357 (2010) 6-35.
[29] K. Zhang, H. Huang, G. Yang, J. Shaw, C. Yip, X.Y. Wu, Characterization of nanostructure of stimuli-responsive polymeric composite membranes, Biomacromolecules, 5 (2004) 1248-1255.
[30] S.P. Nunes, A.R. Behzad, B. Hooghan, R. Sougrat, M. Karunakaran, N. Pradeep, U. Vainio, K.-V. Peinemann, Switchable pH-responsive polymeric membranes prepared via block copolymer micelle assembly, ACS nano, 5 (2011) 3516-3522.
[31] A. Tufani, G.O. Ince, Smart membranes with pH-responsive control of macromolecule permeability, Journal of Membrane Science, 537 (2017) 255-262.
[32] X.-X. Fan, R. Xie, Q. Zhao, X.-Y. Li, X.-J. Ju, W. Wang, Z. Liu, L.-Y. Chu, Dual pH-responsive smart gating membranes, Journal of Membrane Science, 555 (2018) 20-29.
[33] J. Ma, H.M. Andriambololona, D. Quemener, M. Semsarilar, Membrane preparation by sequential spray deposition of polymer PISA nanoparticles, Journal of Membrane Science, 548 (2018) 42-49.
[34] W.D. Mulhearn, D.D. Kim, Y. Gu, D. Lee, Facilitated transport enhances spray layer-by-layer assembly of oppositely charged nanoparticles, Soft Matter, 8 (2012) 10419-10427.
[35] Z. Mouline, M. Semsarilar, A. Deratani, D. Quemener, Stimuli responsive nanostructured porous network from triblock copolymer self-assemblies, Polymer Chemistry, 6 (2015) 2023-2028.
[36] L. Upadhyaya, M. Semsarilar, S. Nehache, D. Cot, R. Fernández-Pacheco, G. Martinez, R. Mallada, A. Deratani, D. Quemener, Nanostructured Mixed Matrix Membranes from Supramolecular Assembly of Block Copolymer Nanoparticles and Iron Oxide Nanoparticles, Macromolecules, 49 (2016) 7908-7916.
[37] L. Upadhyaya, M. Semsarilar, R. Fernández-Pacheco, G. Martinez, R. Mallada, I.M. Coelhoso, C.A. Portugal, J.G. Crespo, A. Deratani, D. Quemener, Nano-structured magneto-responsive membranes from block copolymers and iron oxide nanoparticles, Polymer Chemistry, 8 (2017) 605-614.
[38] M. Semsarilar, V. Ladmiral, A. Blanazs, S.P. Armes, Cationic Polyelectrolyte-Stabilized Nanoparticles via RAFT Aqueous Dispersion Polymerization, Langmuir, 29 (2013) 7416-7424.
[39] D.A. Mbeh, L.K. Mireles, D. Stanicki, L. Tabet, K. Maghni, S. Laurent, E. Sacher, L.H. Yahia, Human alveolar epithelial cell responses to core–shell superparamagnetic iron oxide nanoparticles (SPIONs), Langmuir, 31 (2015) 3829-3839.
[40] N. Miguel-Sancho, O. Bomatí-Miguel, G. Colom, J.P. Salvador, M.P. Marco, J. Santamaría, Development of Stable, Water-Dispersible, and Biofunctionalizable Superparamagnetic Iron Oxide Nanoparticles, Chemistry of Materials, 23 (2011) 2795-2802.
[41] R.W. Baker, Membrane technology and applications, 2nd ed., John Wiley & Sons, Ltd, 2004.
[42] M. Guerre, M. Semsarilar, C. Totée, G. Silly, B. Améduri, V. Ladmiral, Self-assembly of poly(vinylidene fluoride)-block-poly(2-(dimethylamino)ethylmethacrylate) block copolymers prepared by CuAAC click coupling, Polymer Chemistry, 8 (2017) 5203-5211.